Transport of 1-μm Latex Particles in *Pseudomonas aeruginosa* Biofilms

William J. Drury,* Philip S. Stewart,† and William G. Characklis‡
Center for Interfacial Microbial Process Engineering, Montana State University, Bozeman, Montana 59717-0398

Received September 9, 1992/Accepted January 21, 1993

Fluorescent latex microbeads added to a *Pseudomonas aeruginosa* biofilm as tracers of particle movement penetrated the biofilm and remained in it much longer than predicted by a model of advective displacement due to cell growth. Beads with a nominal diameter of 1 μm that were added in the bulk fluid became distributed throughout the biofilm depth. Some microbeads penetrated to the substratum within the 24-h bead addition period. The biofilms had a mean thickness of approximately 34 μm but have been previously shown to be quite rough. Measured rates of bead release from the biofilm corresponded to first order time coefficients of 0.01–0.03 h^{-1}. These bead release rates were approximately an order of magnitude less than the predicted time scale of advective transport, which is just the experimentally measured specific cellular growth rate of 0.15 h^{-1}. Computer simulations of bead transport using the biofilm model BIOSIM were compared with bead release rate data and with bead position distributions within the biofilm as determined by microscopic examination of thin cross sections of embedded biofilm. The model predicted much faster release of beads from the biofilm than actually occurred. It is hypothesized that both the ability of beads to penetrate the biofilm and the unexpectedly low advective displacement velocity of particles in the biofilm were due to the rough nature of the biofilm.

Key words: biofilm • particle • *Pseudomonas aeruginosa* • transport • roughness

INTRODUCTION

This article examines the transport of particulate species within microbial biofilms. Particulate constituents of a biofilm can include microbial cells, extracellular polymers produced by the cells, and inert particles captured by or generated within the biofilm. While the transport of dissolved species in biofilms has been studied extensively, the transport of biofilm particulate constituents has been largely neglected. Transport of dissolved species is thought to occur primarily by molecular diffusion through the aqueous intracellular matrix of the biofilm. The interaction between diffusion and reaction in the biofilm, which gives rise to concentration gradients, is widely recognized as a characteristic feature of biofilms that distinguishes these systems from situations where microbial growth is planktonic. Because transport of microbial cells is thought to be one of the fundamental processes determining population dynamics in a microbial biofilm, it is possible that particulate transport is as important in defining biofilm ecology as transport of soluble species is in defining biofilm chemistry.

Particulate dynamics in a biofilm are thought to be governed by the interaction of microbial growth, advective transport, and attachment and detachment processes.[4,9] The conversion of soluble substrates to cells and extracellular polymeric substances (EPSs) creates particulate volume. This volume increase drives advection of the particulate constituents of the biofilm. The biofilm may expand laterally, filling in holes or pores, or it may expand away from the substratum, growing in thickness. Biofilm expansion resulting from growth is normally balanced by detachment processes, which transfer biomass from the biofilm to the fluid around the film.

In existing mathematical formulations of these ideas, growth and advection occur within the biofilm, whereas detachment and attachment are treated as boundary conditions, that is, they occur only at the surface of a uniformly thick biofilm. According to these models, the ability of a microbial species to persist at any point within the biofilm depends on the local balance of growth, which produces new cell mass, and advection, which carries cell mass away. Such models can correctly predict the stratification of microbial species that can occur in mixed population biofilms.

The purpose of this research was to obtain direct experimental evidence of particulate advection in a biofilm and use these data to evaluate the adequacy of the growth–advection conceptual model of biofilm population dynamics. Advection of bacterial cells has been experimentally observed in special immobilized cell reactors by pulse-chase radiolabeling of biomass with $^{35}SO_4^-$ followed by autoradiography of reactor cross sections.[12,24] To our knowledge, particulate advection has not been directly observed in natural biofilm systems. We used fluorescent latex microbeads as particulate tracers and compared their fate in a *Pseudomonas aeruginosa* biofilm with the predictions of an existing mathematical model.

* Current address: Environmental Engineering and Natural Sciences Divison, Montana College of Mineral Sciences and Technology, Butte, MT 59701.
† To whom all correspondence should be addressed.
‡ Deceased.

CCC 0006-3592/93/010111-07

THEORY

Advective velocities in biofilms have been modeled by writing a differential material balance on particulate species in the biofilm.[9,12,24] Using such a balance, the change in particulate concentrations in biofilm can be described by the partial differential equation

$$\frac{\partial X_i}{\partial t} = -\nabla(vX_i) + r_i \quad (1)$$

This equation equates the rate of accumulation of a particulate species to the difference between the rates that it is advected and created. It neglects the possibility of diffusive-like transport of particles.[9,13]

Several assumptions are normally employed to simplify solution of Equation (1). These include (a) the biofilm is adequately described by a one-dimensional model, (b) the volume fraction of biofilm occupied by water (ϵ_l) is constant, (c) the densities of the particulate species (ρ_i) are constant, and (d) all particulate constituents have a locally equal displacement velocity.[9] With these assumptions, an equation for the advective velocity can be derived by summing the balances on all particulate species:

$$\frac{dv}{dz} = \frac{1}{1 - \epsilon_l} \sum_N \frac{r_i}{\rho_i} \quad (2)$$

Equations (1) and (2) can be solved once suitable initial and boundary conditions are specified.[9] The initial condition describes the profiles of the various particulate species over biofilm depth:

$$\text{at } t = 0, \qquad X_i(z) = X_{i0}(z) \quad (3)$$

Typical boundary conditions require that the velocity be zero at the substratum,

$$\text{at } z = 0, \qquad v = 0 \quad (4a)$$

and specify a flux matching condition at the biofilm surface,

$$\text{at } z = L_f, \qquad v = v_d \quad (4b)$$

where v_d is the detachment rate expressed as a velocity.

An interesting simplification results for a binary population biofilm containing one growing and one nongrowing species if attention is focused on the substratum. The advective velocity is zero at the substratum. If the growing population is at steady state at this point and the nongrowing population is relatively dilute, then it can be shown that

$$\frac{dX_n}{dt} = -\mu_{z=0} X_g \quad (5)$$

where X_n is the concentration of the nongrowing particulate and X_g is the concentration of the growing particulate. Equations (1)–(4) were solved in this work using the commercially available biofilm model BIOSIM.[18,29] The program also solves the reaction–diffusion problem for dissolved species. Reaction kinetics were described by a double Monod dependence on glucose and oxygen concentrations. Extracellular polymer formation by both growth-associated and non-growth-associated pathways was considered.[19]

MATERIALS AND METHODS

Experimental System

Monopopulation *Pseudomonas aeruginosa* biofilms were grown in a rotating annular reactor under turbulent flow conditions. The reactor volume was 5.75×10^{-4} m^3. A flow rate of 2.3×10^{-3} m^3 h^{-1} was used, giving a hydraulic retention time of 0.25 h. The reactor contained 12 removable coupons to allow biofilm sampling. Bacteria were grown aerobically on a defined mineral salts, phosphate buffered medium,[7] with glucose being the limiting nutrient and the only carbon and energy source.

Microbead Characteristics

Latex microbeads (Polysciences, model 15702) had a nominal diameter of 1 μm, approximating the size of a bacterial cell. The beads had a specific gravity of 1.05 and a negative surface charge. A fluorescent dye incorporated into the beads during manufacture made them easy to distinguish under the microscope when illuminated with epifluorescent light. The beads were not biodegradable nor soluble. Bead solutions were autoclaved for 0.33 h before their addition to the reactor.

Analytical Methods

Biofilm was sampled at 24-h intervals. Wet biofilm thickness was measured microscopically,[1] with 5–10 measurements made per sample. Biofilm from a measured area was scraped into a variable volume of phosphate buffered water and homogenized. Bead and cell counts were total direct counts.[10] Samples (variable volumes) for cell counts were added to an equal volume of Hoechst 33342 stain (100 μM), vortexed and stored in the dark

Table I. Experimental protocols and measured bead release and cell growth rates.

Experiment	Period between inoculation and bead addition (h)	Average L_f at end of bead addition (μm)	Length of bead addition (h)	α (h^{-1})	μ (h^{-1})
A-1	0	2.0	24	0.0097 ± 0.0019	0.19
A-2	0	2.2	24	6.0×10^{-5} ± 0.0038	0.20
B-1	120	30	24	0.0212 ± 0.0030	0.083
B-2	120	35	24	0.0306 ± 0.0016	0.11
B-3	120	18	0.14	−0.0011 ± 0.0025	—

for 1–24 h. Bead samples were not stained. The sample, or an aliquot, was filtered through a 0.2-μm black membrane filter and observed under an Olympus BH-2 microscope using epifluorescent light. Particles were counted by an image analysis computer program using either a Cambridge/Olympus hardware and software package or an American Innovision package. Bead number densities were converted to mass densities using the manufacturer's reported bead diameter and specific gravity.

Biofilm samples were dehydrated, embedded in plastic, and cut into 2.5-μm-thick cross sections with a microtome.[7] The thin sections were examined with an Olympus BH-2 microscope using simultaneous transmitted white and epifluorescent light, with distance measurements made with the Olympus microscope and the American Innovision Videometric 150 image analysis system. Distances were measured along a normal to the substratum to beads and to the biofilm–bulk water interface where beads were located. Microbead profiles were constructed from the distances measured on thin cross sections. Bead locations were grouped into 1-μm intervals, and the frequencies were converted to concentrations using the independently measured areal bead concentrations.

Additional experimental details and an evaluation of the use of fluorescent microbeads as a tool to study particle–biofilm interactions are related elsewhere.[6,7]

RESULTS

Two experimental designs were used to study biofilm–particle interactions. These differed in the biofilm age at which tracer particles were added. Beads were added to either nascent biofilms (type A experiments), which were relatively thin, or to mature biofilms (type B experiments), which were an order of magnitude thicker (Table I). Beads were pumped into the reactor for a 24-h period, except in experiment B-3, in which bead addition occurred over a 0.14-h interval. The concentration of beads in the reactor influent during the addition period ranged from approximately 3×10^{12} to 7×10^{14} beads m^{-3}.[7] In both types of experiments, beads added in the bulk fluid attached to biofilm during the bead addition period.

Beads entrapped in the biofilm were slowly released back into the bulk after the end of the bead addition period (Fig. 1). An apparent first order release rate coefficient α was calculated from the data by fitting the empirical equation

$$X_f(z,t) = X_{f0}e^{-\alpha t} \qquad (6)$$

In this equation, X_{f0} is the initial areal concentration of beads, which was different for each experiment. The fastest release rate (α) was approximately 0.03 h^{-1} (Table I).

Embedded biofilm specimens were cross-sectioned and examined microscopically. Biofilm thicknesses measured from the thin cross sections were comparable to those determined optically on fresh biofilm samples but did not always agree well (Table II). Thicknesses measured from cross sections were similar to or greater than thicknesses measured on fresh biofilm. Thicknesses measured from cross sections represent the average of data taken at one point in the biofilm, whereas optically measured thicknesses were the average of data from 5–10 distinct biofilm locations. As related elsewhere,[25] biofilm thickness measurements were broadly distributed, suggesting a rough biofilm.

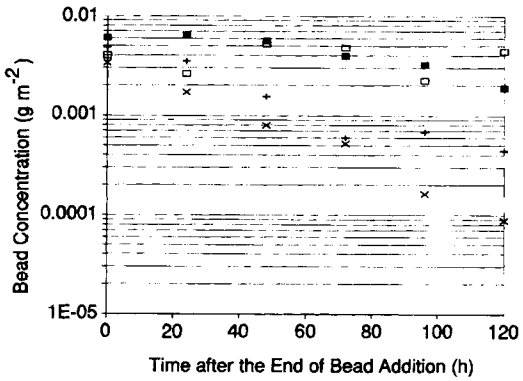

Figure 1. Biofilm microbead concentrations over time for duplicate experiments with nascent (■, □) and mature (+, ×) biofilms.

The spatial distribution of beads within the biofilm was measured by microscopic examination of embedded cross sections of biofilm samples. Microbead concentration profiles were constructed for the nascent biofilm experiment A-1 from samples taken 24.2, 48.2, and 96.2 h after the end of bead addition. Bead concentrations were higher near the substratum than near the biofilm surface in all three profiles (Fig. 2). Bead concentrations generally decrease over time. The highest measured concentration of beads was about 1500 g m^{-3}. This corresponds to a volume fraction of approximately 1.4×10^{-3}. The beads are, therefore, a relatively dilute component of the biofilm.

Bead concentration profiles were also constructed for the mature biofilm experiments B-2 (Fig. 3) and B-3 (Fig. 4). Forty-five minutes after the end of bead addition in experiment B-2, the greatest concentrations of beads occur 25–35 μm from the substratum. This suggests that the majority of beads were near the biofilm surface, since the average film thickness was 34 μm (Table II). A day

Table II. Biofilm thicknesses.

Experiment	Time of sample (h)	Fresh biofilm sample (μm)	Embedded biofilm sample (μm)
A-1	48	7.5 ±2.0	12.7 ±6.2
	72	14 ±3.4	13.7 ±6.3
	120	26 ±3.3	26.2 ±11.1
B-2	144	35 ±8.8	33.0 ±11.5
	168	11 ±7.4	70.9 ±61.4
B-3	120	18 ±6.5	37.2 ±10.0
	122.9	—	39.8 ±6.2
	128.9	—	39.2 ±11.1
	144	19 ±5.0	33.3 ±11.2
	192	13 ±3.2	37.3 ±9.6

Values are mean ± one standard deviation in thickness measurements.

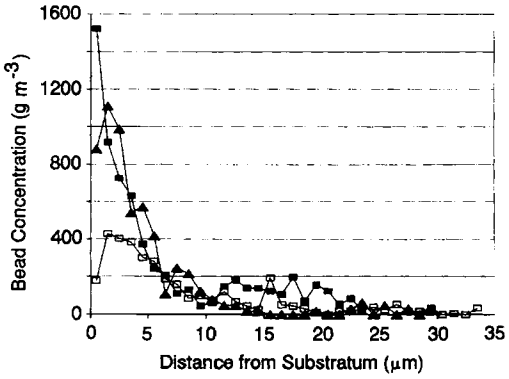

Figure 2. Profiles of microbead concentrations over biofilm depth in experiment A-1 at 24 (■), 48 (▲), and 96 (□) h after the end of bead addition.

later (24.6 h after the end of bead addition) the bead concentration profile describes a gradient that decreases toward the biofilm surface. Bead concentration profiles obtained from experiment B-3 are similar to those seen in experiment B-2 for short times (<10 h) after the end of bead addition (Fig. 4a). At longer times, the modes of the bead distributions drift slowly toward the substratum (Fig. 4b).

The average specific growth rate in the biofilm, μ, was calculated by dividing the overall rate of cell production (cells m^{-2} h^{-1}) by the biofilm areal cell density (cells m^{-2}). The average specific growth rate was approximately 0.15 h^{-1} (Table I). The apparent cellular growth rate at the substratum in experiment A-1 was estimated from the change in bead concentration in the 1-μm interval nearest the substratum by applying Equation (5). The growth rate calculated in this way was 0.030 ± 0.003 h^{-1} for the 72-h period spanned by the profile data.

The computer program BIOSIM was used to predict population dynamics in the biofilm. Parameter values describing the biofilm and the growth and activity of *P. aeruginosa* are listed in Table III. The model predicted cell accumulation and activity well, accurately matching data for areal (biofilm) cell concentration as well as effluent concentrations of glucose and cells.[6] Given that the advective velocity will always be away from the substratum and that the model assumes a uniformly thick biofilm, the model has no capacity to distribute beads over biofilm depth. Because the model could not accommodate the initial movement of beads into the biofilm, a bead profile from a time shortly after the end of bead addition (Fig. 3, 0.75 h profile) was entered as an initial condition. The model was then used to predict the areal concentration and distribution of beads in the biofilm at a later time.

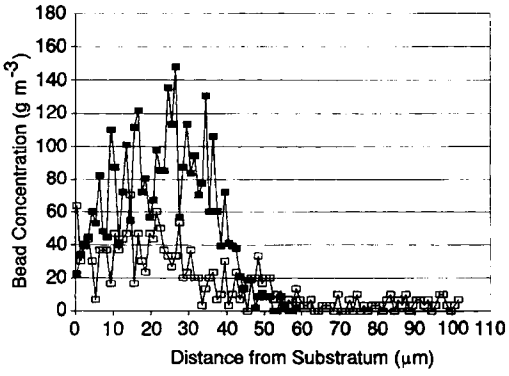

Figure 3. Profiles of microbead concentrations over biofilm depth in experiment B-2 at 0.75 (■) and 24.6 (□) h after the end of bead addition.

When areal bead concentrations in experiments B-1 and B-2 were thus simulated, the model predicted a significantly more rapid rate of release than was observed (Fig. 5). To evaluate the magnitude of the discrepancy, the values of the maximum growth rate and the non-growth-associated polymer formation coefficient used in the simulation were divided by 20. The factor of 20 was arrived at by trial and error. The intent of this exercise was not to contrive a fit between the data and theory but to assess the magnitude of the failure of the model. The model did predict areal bead concentrations well using the reduced growth rates (Fig. 5).

For this simulation, the cell and polymer growth rates, 0.013 and 0.014 h^{-1}, respectively, summed to 0.027 h^{-1}. This rate is close to the bead dilution rate near the substratum observed in experiment A-1 (0.030 h^{-1}) and to the empirical first order release rates for experiments B-1 and B-2 (average 0.026 h^{-1}). When the full growth rate was used to model areal bead concentrations in the nascent biofilm experiments A-1 and A-2, the model again overpredicted the rate of bead release (data not shown).

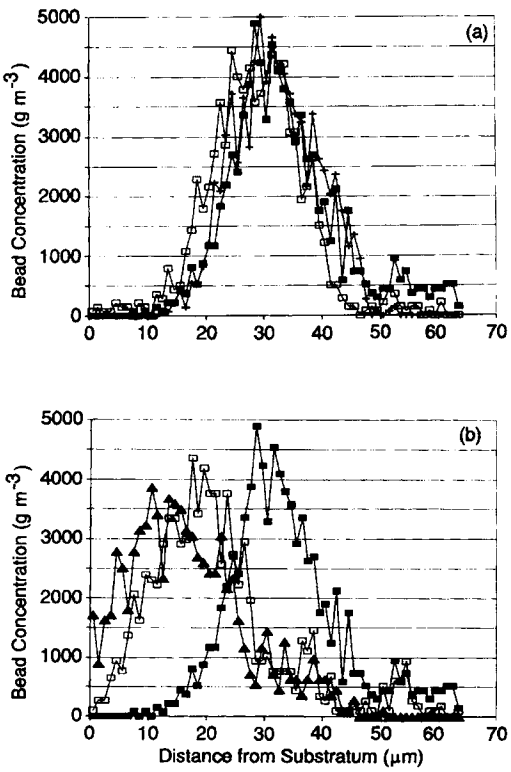

Figure 4. Profiles of microbead concentrations over biofilm depth in experiment B-3: (a) profiles at 0.05 (■), 2.9 (+), and 8.9 (□) h after the end of bead addition; (b) profiles at 0.05 (■), 23.9 (□), and 71.9 (▲) h after the end of bead addition. The profile at 0.05 h is shown in both graphs as a comparative reference.

Table III. Parameter values for biofilm modeling.

Coefficient	Value	Reference
μ_{max}	0.37 h^{-1}	5
K_s	1.6 g m^{-3}	5
K_{O_2}	0.1 g m^{-3}	14
$Y_{x/s}$	0.24 g g^{-1}	21
$Y_{p/s}$	0.41 g g^{-1}	21
$Y_{x/o}$	0.21 g g^{-1}	19, 27
k_p	0.36 g g^{-1}	22
k_p'	2.40 g g^{-1} d^{-1}	22
ϵ_l	0.90	6
D_f/D	0.90	30
D_s	5.8×10^{-5} m^2 d^{-1}	17
D_{O_2}	2.0×10^{-4} m^2 d^{-1}	17
ρ_x	118,000 g m^{-3}	19
ρ_p	110,000 g m^{-3}	6
L_f	3.4×10^{-5} m	25
L_L	1×10^{-6} m	6
C_s	15 g m^{-3}	6
C_{O_2}	7 g m^{-3}	6
A	0.19 m^2	6
V	5.75×10^{-4} m^{-3}	6
Q	2.3×10^{-3} m^{-3} h^{-1}	6

Better predictions were obtained using the reduced growth rate.

The model did not predict the shape of bead distributions well (Fig. 6). Experimentally measured distributions from mature biofilms had modes that moved toward the substratum, if at all, and that maintained significant concentration gradients. BIOSIM generated distributions had modes that moved toward the biofilm surface while the distribution progressively flattened, tending toward a zero slope. Decreasing the specific growth rate did not reconcile the differences between the model and the data (Fig. 6b).

DISCUSSION

Microbeads added in the bulk liquid become distributed throughout the biofilm depth (Figs. 2 and 3). This indicates that a transport mechanism exists that can move particles into the biofilm. Current mathematical models of biofilms allow for particle attachment at the surface of the film but incorporate no mechanism to explain particle penetration into the biofilm in a direction opposite that of growth-driven advection. Three possible physical mechanisms to explain this phenomenon are considered below. These are inertial transport, diffusion, and surface roughness.

It is conceivable that momentum obtained by beads from fluid motion of the bulk water is sufficient to drive their penetration into the biofilm. Momentum in a direction normal to the plane of the biofilm could be derived from either centripetal acceleration associated with the annular flow or from turbulent fluid motion. The relative importance of inertial forces in bead transport can be evaluated by calculating a Reynolds number. The radial velocity calculated from a balance of viscous drag and centripetal acceleration is approximately 0.018 m h^{-1}, yielding a particle Reynolds number of 5.5×10^{-6}. The fluid velocity perpendicular to the reactor wall due to turbulence is estimated to be 0.11 m h^{-1},[2,6] resulting in a particle Reynolds number of 3.5×10^{-5}. In both cases, the very small Reynolds numbers indicate that viscous forces strongly dominate inertial forces. It appears, therefore, that inertial penetration of beads into the biofilm is unlikely.

Particles might penetrate the biofilm by diffusive transport through the biofilm matrix. From the Stokes–Einstein equation, the diffusion coefficient of beads in water is estimated to be 1.75×10^{-9} m^2 h^{-1} at 25°C. The time scale for beads to traverse the 35-μm thickness of a mature biofilm ($L_f^2 D^{-1}$) would thus be approximately 0.7 h. If this were realistic, diffusion could explain the observed extent of penetration of the biofilm in 11 min to 24 h (Figs. 3 and 4). It is unlikely, however, that beads can actually diffuse at all through the gel-like structure of the biofilm polymer. Electron micrographs of biofilms suggest that the polymer network has a spacing significantly smaller than the 1-μm microbeads.[3,11,16] Furthermore, if beads were to diffuse in this manner, one would expect a rapid release of beads from the biofilm after the end of the bead addition period as beads diffused back out of the film. No such release is observed.

The most plausible explanation for "penetration" of beads into the biofilm is that the biofilm surface is actually quite rough, so that beads are able to diffuse into the biofilm interior through water-filled pores. The term "rough" is meant to convey that the thickness of the biofilm is variable and that the thickness changes over lateral distance scales comparable to or shorter than the mean thickness. The existence of pores or surface irregularities in biofilms has been observed in diverse systems,[8,15,20,26] and we have discussed elsewhere the apparent roughness of the *Pseudomonas* biofilms grown in our reactors.[25] The roughness of the biofilm is revealed by the relatively large variation in measured thicknesses (Table II). The coefficients of variation of all of the thickness measurements reported in

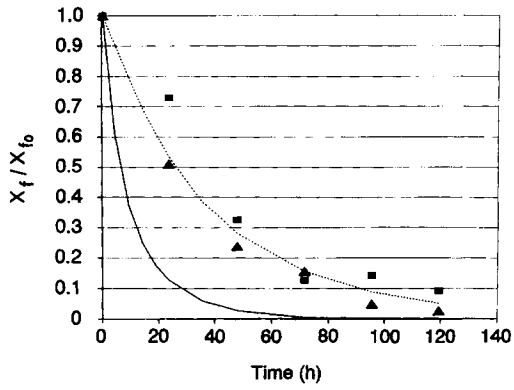

Figure 5. Nondimensionalized areal bead concentrations. Data are from experiments B-1 (■) and B-2 (▲). Simulations are for full (——) and reduced (·····) growth rates. The time scale is hours after the end of bead addition.

Table II average 35%. The variability of biofilm thickness is also suggested by the broad distribution of bead measured experimentally (Figs. 3 and 4); beads can be found at distances twice or even three times the mean biofilm thickness. To recap this explanation, beads permeate the biofilm and become distributed throughout its depth simply because the biofilm is rough.

The retention time for microbeads in biofilm was significantly longer than the turnover time implied by the specific cellular growth rate (Table I). Whereas the microbial growth rate averaged 0.15 h^{-1}, the observed first order release rate of beads never exceeded 0.031 h^{-1}. The latter value is consistent with the rate of bead dilution at the substratum observed in experiment A-1 (0.030 h^{-1}). Restating this discrepancy in terms of the advective displacement model of biofilm dynamics, the apparent advection rate was much slower than the rate suggested by the specific growth rate. The failure of the computer model to match experimental data and the partial compensation achieved by artificially reducing the growth rate (Fig. 5) are consistent with the interpretation that advection was slower than growth.

We hypothesize that biofilm roughness is responsible for the observed reduction in particulate advection velocity within the biofilm. Biofilm roughness could reduce advection in two ways. First, if the biofilm has a rough surface, then advection of particulate mass can occur in directions parallel to the substratum. This lateral filling in of pores would not contribute to advection perpendicular to the substratum. A particle that attaches in a pore, such as the microbeads used in this study, could become entrapped in the biofilm matrix as cell growth fills in the pore. Second, pores could provide a "back door" for detaching biomass to leave the biofilm and thereby reduce the net generation of biomass volume within the film. Since the microbeads are retained longer in the biofilm than are the microorganisms, it appears, in this case, that the inert beads detach less readily than do growing cells. In summary, biofilm roughness could thus explain both the penetration of tracer microbeads into the biofilm and their prolonged retention.

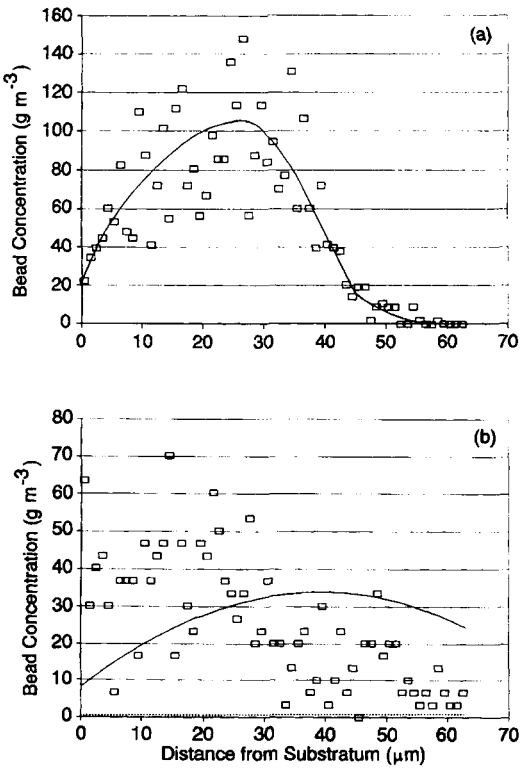

Figure 6. Bead profiles from experiment B-2 at 0.75 (a) and 24.6 (b) h after the end of bead addition. The symbols (□) indicate experimental data. The solid line indicates the assumed initial condition in (a) and the predicted distribution for $\mu = 0.025\ h^{-1}$ in (b). The dashed line indicates the simulated profile in (b) for $\mu = 0.15\ h^{-1}$.

These experimental results suggest that the conceptual model of the biofilm that treats it as a uniformly thick aggregate may be inadequate for describing biofilm population dynamics. The authors of the BIOSIM model recognized this limitation to their construct.[9,28] Improved understanding of biofilm population dynamics will probably require a new conceptual description of the biofilm that incorporates the inherent heterogeneities in its structure. Experimental and theoretical methods for characterizing biofilm roughness are needed, as are new approaches to describing attachment and detachment that occurs "within" the biofilm. Since inert and viable particles probably experience advection identically, labeled inert particles should continue to prove useful in the investigation of biofilm population dynamics.

In summary, this work provides evidence that transport of particles into and out of a biofilm cannot be adequately described by a conceptual model that balances growth and advection in a uniformly thick biofilm. Biofilm roughness is the most likely explanation of this failure. Biofilm roughness probably explains the penetration of particles into the biofilm and may be the explanation for their relatively slow release. Although this work points to an important role for biofilm roughness, it sheds no light on the mechanisms that generate or sustain it. A hypothesis regarding one such mechanism is that thickness variation results when multicellular aggregates detach from the biofilm.[23] Additional theoretical and experimental work is required to address the ways in which roughness arises and how it impacts biofilm activity and dynamics.

CONCLUSIONS

Fluorescently tagged 1-μm latex beads were used as tracers to investigate particle transport in *P. aeruginosa* biofilms grown in laboratory annular reactors. Beads added to the reactor in the bulk fluid entered the biofilm and became distributed throughout the biofilm depth. The rate of particulate advection within the biofilm, as determined from measurements of bead position and number in the biofilm, was an order of magnitude slower than predicted by a model that balances growth and advection in a uniformly thick biofilm. The penetration of beads into the biofilm and their slow release were both hypothesized to result from

the thickness variability, or roughness, of the experimental biofilms.

The authors gratefully acknowledge support through Cooperative Agreement ECD-8907039 between the National Science Foundation and Montana State University and the Center Industrial Associates.

NOMENCLATURE

A	surface area for biofilm growth in the reactor (L^2)
C	dissolved species concentration in the reactor influence (ML^{-3})
D	diffusion coefficient in water (L^2t^{-1})
D_f	effective diffusion coefficient for solute in biofilm (L^2t^{-1})
K	half-saturation coefficient for bacterial growth (ML^{-3})
k_p	growth associated polymer formation coefficient ($M_pM_x^{-1}$)
k'_p	non-growth associated polymer formation coefficient ($M_pM_x^{-1}t^{-1}$)
L_f	biofilm thickness (L)
L_L	mass transfer boundary layer thickness (L)
Q	liquid flow rate through the reactor (L^3t^{-1})
r	reaction rate of particulate species (t^{-1})
t	time (t)
v	advective velocity of particulates in the biofilm (Lt^{-1})
v_d	detachment rate expressed as a velocity (Lt^{-1})
V	reactor liquid volume (L^3)
X_i	volume concentration of particulate species i(ML^{-3})
X_{i0}	initial volume concentration of particulate species i(ML^{-3})
X_f	areal particulate concentration (ML^{-2})
X_{f0}	areal particulate concentration immediately after end of bead addition (ML^{-2})
$Y_{i/j}$	yield coefficient of species i on species j (carbon mass basis) ($M_iM_j^{-1}$)
z	spatial coordinate perpendicular to biofilm substratum

Greek symbols

α	bead release rate coefficient (t^{-1})
ϵ_l	volume fraction of liquid to total biofilm volume (dimensionless)
ρ	intrinsic density of particulate species (ML^{-3})
μ	average specific growth rate (t^{-1})
μ_{max}	maximum specific growth rate (t^{-1})

Subscripts

g	growing particulate species
i, j	arbitrary index
n	nongrowing particulate species
O_2	oxygen
p	extracellular polymeric substances
s	glucose
x	cell mass

References

1. Bakke, R., Ollsen, P.Q. 1986. Biofilm thickness measurements by light microscopy. J. Microb. Meth. **5**: 1–6.
2. Beal, S.K. 1970. Deposition of particles in turbulent flow on channel or pipe walls. Nucl. Sci. Eng. **40**: 1–11.
3. Beeftink, H.H., Staugaard, P. 1986. Structure and dynamics of anaerobic bacterial aggregates in a gas lift reactor. Appl. Environ. Microbiol. **52**: 1139–1146.
4. Bryers, J.D., Characklis, W.G. 1982. Processes governing primary biofilm formation. Biotechnol. Bioeng. **24**: 2451–2476.
5. Characklis, W.G. 1990. Kinetics of microbial transformations. pp. 233–264 In: W.G. Characklis and K.C. Marshal (eds.), Biofilms. Wiley, New York.
6. Drury, W.J. 1992. Interactions of 1 μm latex microbeads with biofilms. Unpublished Ph.D. thesis, Montana State University, Bozeman, MT.
7. Drury, W.J., Characklis, W.G., Stewart, P.S. Interactions of 1 μm latex particles with *Pseudomonas aeruginosa* biofilms. Water Res., in press.
8. Eighmy, T.T., Maratea, D., Bishop, P.L. 1983. Electron microscopic examination of wastewater biofilm formation and structural components. Appl. Environ. Microbiol. **45**: 1921–1931.
9. Gujer, W., Wanner, O. 1990. Modeling mixed population biofilms. pp. 397–444. In: W.G. Characklis and K.C. Marshall (eds.), Biofilms. Wiley, New York.
10. Hobbie, J.E., Dalen, R.J., Jasper, S. 1977. Use of nucleopore filters for counting bacteria by fluorescence microscopy. Appl. Environ. Microbiol. **35**: 858–862.
11. Jones, H.C., Roth, I.L., Sanders, W.M. 1969. Electron microscopic study of a slime layer. J. Bacteriol. **99**: 316–325.
12. Karel, S.F., Roberston, C.R. 1989. Autoradiographic determination of mass-transfer limitations in immobilized cell reactors. Biotechnol. Bioeng. **34**: 320–336.
13. Kissel, J.C., McCarty, P.L., Street, R.L. 1984. Numerical simulation of mixed-culture biofilm. J. Environ. Eng. **110**: 393–411.
14. Lewandowski, Z., Walser, G., Characklis, W.G. 191. Reaction kinetics in biofilms. Biotechnol. Bioeng. **38**: 877–882.
15. Mack, W.N., Mack, J.P., Ackerson, A.O. 1975. Microbial film development in a trickling filter. Microb. Ecol. **2**: 215–226.
16. MacLeod, F.A., Guiot, S.R., Costerton, J.W. 1990. Layered structure of bacterial aggregates produced in an upflow anaerobic sludge bed and filter reactor. Appl. Environ. Microbiol. **56:** 1598–1607.
17. Perry, R.H., Chilton, C.H. 1973. Chemical engineer's handbook, 5th ed. McGraw-Hill, New York.
18. Reichert, P., Ruchti, J., Wanner, O. 1989. BIOSIM—Interactive program for the simulation of the dynamics of mixed culture biofilm systems on a personal computer. Swiss Federal Institute for Water Resources and Water Pollution Control, Swiss Federal Institutes of Technology, CH-8600, Dubendorf, Switzerland.
19. Robinson, J.A., Trulear, M.G., Characklis, W.G. 1984. Cellular reproduction and extracellular polymer formation by *Pseudomonas aeruginosa* in continuous culture. Biotechnol. Bioeng. **26**: 1409–1417.
20. Robinson, R.W., Akin, D.E., Nordstedt, R.A., Thomas, M.V., Aldrich, H.C. 1984. Light and electron microscopic examinations of methane-producing biofilms from anaerobic fixed-bed reactors. Appl. Environ. Microbiol. **48**: 127–136.
21. Siebel, M.A. 1987. Binary population biofilms. Unpublished Ph.D. Thesis, Montana State University, Bozeman, MT.
22. Siebel, M.A., Characklis, W.G. 191. Observations of binary population biofilms. Biotechnol. Bioeng. **37**: 778–789.
23. Stewart, P.S. 1993. A model of biofilm detachment. Biotechnol. Bioeng. **41**: 111–117.
24. Stewart, P.S., Karel, S.F., Robertson, C.R. 1991. Characterization of immobilized cell growth rates using autoradiography. Biotechnol. Bioeng. **37**: 824–833.
25. Stewart, P.S., Peyton, B.M., Drury, W.J., Murga, R. 1993. Quantitative observations of heteogeneities in *Pseudomonas aeruginosa* biofilms. Appl. Environ. Microbiol., **59**: 327–329.
26. Switzenbaum, M.S., Eimstad, R.B. 1987. Analysis of anaerobic biofilms. Environ. Technol. Lett. **8**: 21–32.
27. Turakhia, M.H., Characklis, W.G. 1989. Activity of *Pseudomonas aeruginosa* in biofilms: Effect of calcium. Biotechnol. Bioeng. **33**: 406–414.
28. Wanner, O. 1989. Modelling population dynamics. pp. 91–110 In: W.G. Characklis and P.A. Wilderer (eds.), Structure and function of biofilms. John Wiley & Sons, New York.
29. Wanner, O., Gujer, W. 1986. A multispecies biofilm model. Biotechnol. Bioeng. **28**: 314–328.
30. Westrin, B.A., Axelsson, A. 191. Diffusion in gels containing immobilized cells: A critical review. Biotechnol. Bioeng. **38**: 439–446.